

Efficient Piecewise Training of Deep Structured Models for Semantic Segmentation

Guosheng Lin, Chunhua Shen, Ian Reid, Anton van den Hengel

Abstract—Recent advances on semantic image segmentation are achieved by training deep convolutional neural networks (DCNNs) on a large amount of labelled images. On the other hand, structured models such as conditional random fields (CRFs) are an effective tool for labelling tasks, which play an important role in that CRFs can capture the global context of the image as well as local neighbourhood information.

Here we explore contextual information to improve semantic image segmentation by taking advantage of the strength of both DCNNs and CRFs. Specifically, we train CRFs whose potential functions are modelled by fully convolutional neural networks (FCNNs). The resulted deep conditional random fields (DCRFs) are thus able to learn complex feature representations; and during the course of learning, dependencies between the output variables are taken into account. As in conventional DCNNs, the training of our model is performed in an end-to-end fashion using back-propagation. Different from DCNNs, however, inference may be needed at each gradient descent iteration, which can be computationally very expensive since typically millions of iterations are required. To enable efficient training, we propose to use approximate training, namely, piecewise training of CRFs, avoiding repeated inference.

We achieve very competitive results on the PASCAL VOC 2012 dataset for semantic segmentation. Our model is trained on the VOC dataset alone with no extra data; and we achieve an intersection-over-union score of 70.7 on its test set, which outperforms state-of-the-art results. Our superior results particularly highlight the usefulness of the learnt pairwise neighbourhood relations modelled by complex FCNNs.

Index Terms—Conditional Random Field, Deep Convolutional Neural Networks (CNN), Fully Convolutional Networks, Semantic Labelling.



1 INTRODUCTION

The task of semantic image segmentation is to predict a category label for every image pixel, which is an important yet challenging task for image understanding. Recent approaches have applied convolutional neural network (CNNs) [1], [2], [3] to this pixel level labeling task and achieved remarkable success. Among these CNNs based methods, fully convolutional neural networks (FCNNs) [2], [3] become a popular choice for the segmentation task, which have the state-of-the-art performance on semantic segmentation. The main advantage of FCNNs is the computational efficiency for dense prediction and end-to-end style learning.

Contextual information provides important cues for object recognition tasks. Contextual information can be formulated as the compatibility relations between one object and its neighbouring objects or image patches. The compatibility relation is an indication of co-occurrence of visual patterns. For example, a car probably appears right above a road; a glass indicates a dining table. Context can also encode in-compatibility relations, clearly. For example, a car is not likely to be surrounded by sky. Contextual relations are ubiquitous. These relations also

exist in a fine-grained aspect, e.g., the object part-to-part relations, the part-to-object relations, etc. In some cases, contextual information is the most crucial cue when a single object shows great visual ambiguities.

Recent CNNs based segmentation methods often do not *explicitly* model contextual relations. It remains unclear how to effectively capture context evidences in CNNs. We here propose a method that explicitly models the contextual relations using conditional random fields (CRFs). We jointly train FCNNs and CRFs to combine the strength of CNNs on learning powerful feature representations and CRFs on complex relation modeling. Our main contributions are thus as follows.

1. We take advantage of the strength of CNNs on learning representations and CRFs on relation modeling. As in conventional CNNs, the training of our model is performed in an end-to-end fashion using back-propagation. Different from DCNNs, however, inference may be needed at each gradient descent iteration, which can be computationally very expensive since typically millions of iterations are required. To make the computation tractable, we propose to use approximate training, namely, piecewise training of CRFs [4], avoiding repeated inference.
2. We propose a semantic segmentation approach to capture different types of context evidences. Here we explore two types of context evidences: neighbouring patch evidence and background evidence. (1) For learning neighbourhood evidence, we con-

· The authors are with The University of Adelaide, Australia; and Australian Centre for Robotic Vision.

· This research was in part supported by the Data to Decisions Cooperative Research Centre (D2DCRC); C. Shen's participation was in part support by ARC Future Fellowship; I. Reid's participation was in part support by ARC Laureate Fellowship. The authors would like to thank NVIDIA for GPU donation.

struct multiple types of pairwise potential functions for modeling different types of relative position relations, such as “surrounding”, “above” and “below”, etc.

(2) For learning multi-scale background evidence, we develop a network architecture to accept multi-scale image inputs of arbitrary sizes.

1.1 Related work

In the past a few years, CNNs have achieved great success in vision recognition tasks, including large-scale image classification [5], fine-grained classification [6], object detection [6], pose estimation [7] and semantic image segmentation [1], [2], [3].

A number of existing CNNs based methods for segmentation are region proposal based methods [6], [8], which first generate region proposals and then assign category labels to each region. More recently, FCNNs [2], [3], [9] become a popular choice for semantic segmentation, which are capable for efficient feature generation and end-to-end training. FCNNs are also actively studied in other tasks for dense prediction recently, such as image restoration [10], image super-resolution [11] and depth estimations [12], [13]. Our method is built upon fully convolution-style networks.

Combining the strength of CNNs and CRFs for segmentation is also addressed in several concurrent work recently. DeepLab-CRF in [3] trains FCNNs and applies the dense CRFs [14] method as a *post-processing* step. In other words, their method applies CNNs and CRFs separately, while our method jointly trains CNNs and CRFs. The method in [15] extends DeepLab by jointly learning the dense CRFs and CNNs. However, they only learn smoothness pairwise potential functions. Since they consider fully-connected CRFs that rely on mean field approximation, their training procedure is different from ours. Our method learns general pairwise potential functions, and resorts to piecewise CRF training for efficiency. The work in [16] shows that the mean-field algorithm for solving CRF inference can be formulated as recurrent neural networks.

Apart from semantic segmentation, some work addresses the problem of jointly learning CNNs and CRFs for various applications. The recent work in [13], [17] proposes to jointly learn *continuous* CRFs and CNNs for depth estimation from a single image. They focus on continuous value prediction, while our method is for categorical label prediction, and the prediction variables are discrete in nature. The work in [7] combines CRFs and CNNs for human pose estimation. They first train a unary-only model then perform joint unary- and pairwise-term learning as a fine-tuning step. During fine-tuning they simply drop the partition function for a loose approximation. The concurrent work in [18] explores joint training of Markov random fields and deep neural networks for the tasks of predicting words from noisy images and image multi-class classification. They

need to compute the marginals for each gradient decent iteration, which can be computationally very expensive. For the segmentation task which usually involves a large number of nodes and edges, this approach might become impractically slow.

Recent segmentation methods in [2] (FCN) and [19] show significant performance improvements by incorporating multi-scale CNN features. FCN generates multi-scale features from middle layers of CNNs, while our method generates multi-scale feature maps from multi-scale image inputs. The method in [19] is a super-pixel based approach without end-to-end learning. They generate multi-scale features for super-pixels.

2 OVERVIEW OF OUR METHOD

An overview of our method is described in Figs. 2 and 3. Fig. 2 shows an illustration of the training and prediction processes, given one input image. We here define one type of unary potential function and 3 types of pairwise potential functions. Different types of pairwise potential functions capture different types of relative position relations. These 3 types of relative position relations are “surrounding”, “above” and “below”, which are described in Fig. 1. The position relations define the neighborhood connection patterns of one node in the CRF graph. It is expected that pairwise potential functions are able to capture different types of neighborhood evidences. We construct asymmetric potential functions for learning from different types of position relations. Asymmetric potential function is also studied in [21], [22] for modeling object layouts and spatial relations.

Fig. 2 shows how we construct one network for one potential function. An input image is fed into one unary and other 3 pairwise networks (4 networks in total). These networks have the same architecture, but do not share network parameters. During the course of training, all network outputs go through a CRF loss layer. When performing prediction, a segmentation mask is produced by solving the CRF MAP inference.

Fig. 3 shows the details of one unary/pairwise network. The left part in the figure is to generate multi-scale feature maps. An input image is first resized into 3 scales, then each rescaled image goes through 6 convolution blocks (“Network Part-1”) to output 3 feature maps. Note that convolution layers are able to accept input images of arbitrary sizes; and the resulted 3 feature maps are of different sizes.

The CRF graph is constructed based on the largest feature map. The 2 smaller feature maps are upscaled to the size of the largest feature map using nearest-neighbour interpolation, same as the “convolution maps upsampling” operator in Liu et al. (see Fig. 6 of [17]). With these features maps, we generate features for each node or pairwise connection (edge) in the CRF graph. Following the work in [23], we concatenate the corresponding node features to get the pairwise features for each edge of the CRF graph, which results in asymmetric potential

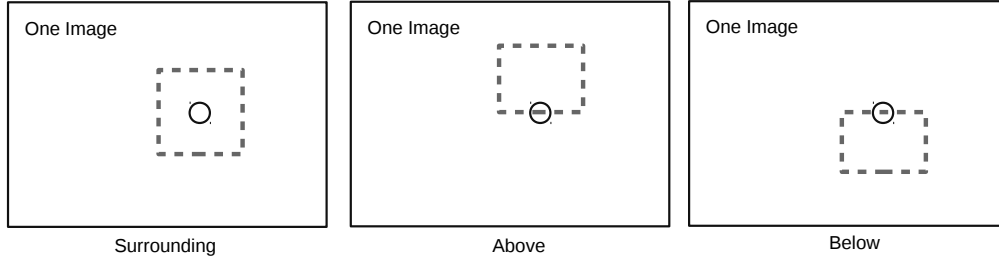


Fig. 1 – An illustration of different types of relative position relations, each of which corresponds to a type of pairwise potential function. A node is connected to all other nodes which lie within the dash box.

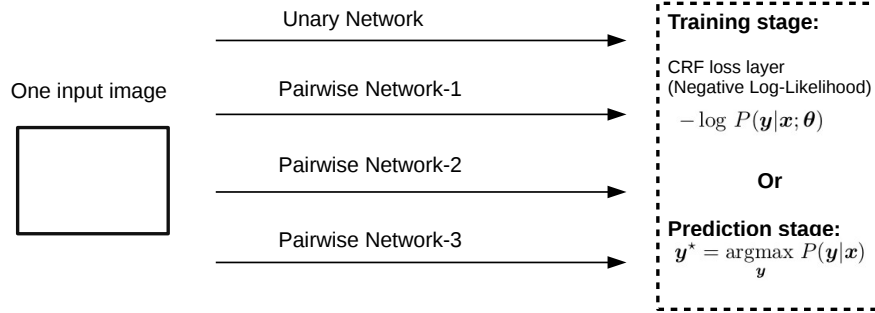


Fig. 2 – An illustration of the training and prediction process, given an input image. An input image is fed into one unary and multiple (in this case, three) pairwise networks. During the training, all network outputs go through a CRF loss layer. When performing prediction, a segmentation prediction is produced by solving the CRF-MAP inference. Details of an unary/pairwise network are shown in Fig. 3.

One Unary/Pairwise Network:

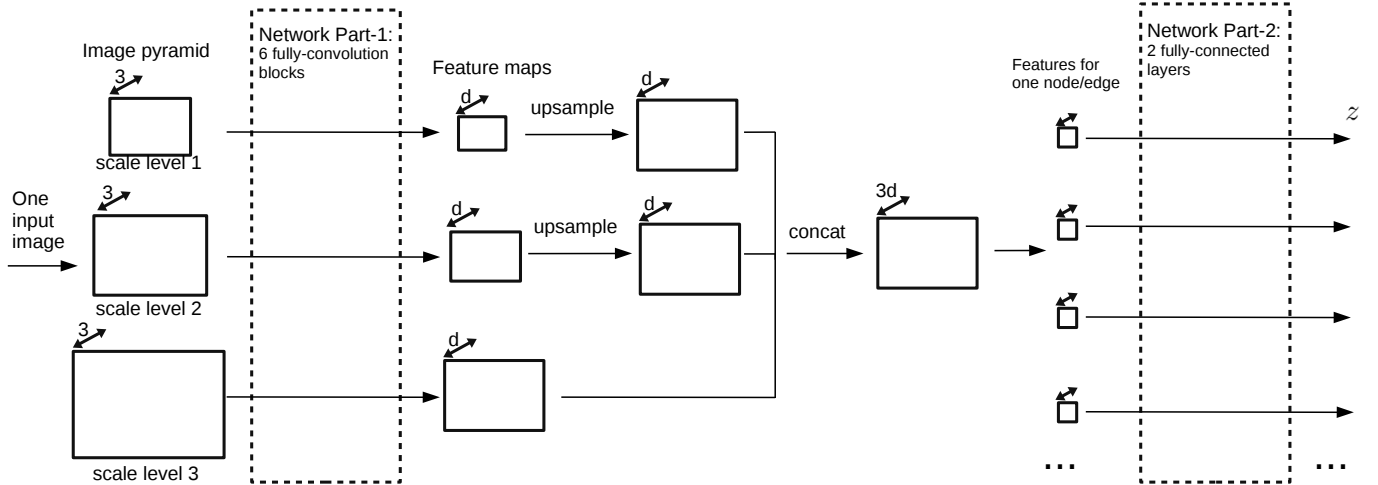


Fig. 3 – An illustration of the details of one unary or one pairwise network. An input image is first resized into 3 scales, then each resized image goes through 6 convolution blocks to output 3 feature maps. Then a CRF graph is constructed and node or edge features are generated from the feature maps. Node or edge features go through a shared fully-connected network to generate the unary/pairwise network outputs. Finally the network outputs are fed into a CRF loss function in the training stage, or an MAP inference objective for prediction.

functions. Finally the features for each node/edge go through 2 fully connected layers (“Network Part-2”) to generate the unary/pairwise network output.

The detailed configuration of networks is described in Fig. 4. “Network Part-1” contains 6 convolution blocks. The configuration of the first 5 convolution blocks is based on the VGG-16 model [20]. The configuration of the first layer in the 6th convolution block is initialised using the first fully connected layer of the VGG-16 model trained on ImageNet.

In the next section, we describe our approach for CRF

learning and prediction in detail.

3 DEEP CONVOLUTIONAL CRFS

We denote by $x \in \mathcal{X}$ one input image and $y \in \mathcal{Y}$ the labeling mask. The energy function is denoted by $E(y, x; \theta)$ which describes the compatibility of the input-output pair. The parameters of all unary and pairwise networks are denoted by θ which we need to learn. The conditional distribution of the prediction for one image

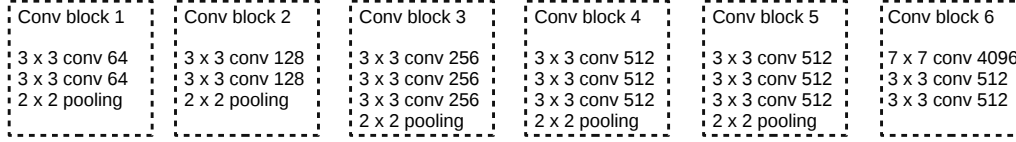
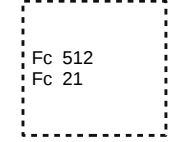
Network Part-1:**Network Part-2:**

Fig. 4 – The detailed configuration of networks. “Network Part-1” and “Network Part-2” are described in Fig. 3. Here “Network Part-1” contains 6 convolution blocks. The configuration of the first 5 convolution blocks is inspired by the VGG-16 model [20].

is formulated as follows:

$$P(\mathbf{y}|\mathbf{x}) = \frac{1}{Z(\mathbf{x})} \exp[-E(\mathbf{y}, \mathbf{x})]. \quad (1)$$

Here Z is the partition function, which is defined as:

$$Z(\mathbf{x}) = \sum_{\mathbf{y}} \exp[-E(\mathbf{y}, \mathbf{x})]. \quad (2)$$

The energy function is typically formulated by a set of unary and pairwise potential functions, which is written as:

$$E(\mathbf{y}, \mathbf{x}) = \sum_{U \in \mathcal{U}} \sum_{p \in \mathcal{N}_U} U(y_p, \mathbf{x}) + \sum_{V \in \mathcal{V}} \sum_{(p,q) \in \mathcal{S}_V} V(y_p, y_q, \mathbf{x}). \quad (3)$$

Here U is a unary potential function which is defined on nodes; To make the exposition general, here we consider multiple types of unary potential functions. \mathcal{U} is the set of all types of unary potential functions. Likewise, V is the pairwise factor function which is defined on edges. \mathcal{V} is the set of all types of pairwise potential functions. \mathcal{S}_V is a set of pairwise relations for the potential function V .

In our experiments, we have defined one type of unary potential function and 3 types of pairwise potential functions to capture different types of neighborhood evidences. We aim to jointly learn all $U \in \mathcal{U}$ and $V \in \mathcal{V}$ in a unified CNN framework.

3.1 Unary potential functions

We formulate the unary potential function as follows:

$$U(y_p, \mathbf{x}; \theta_U) = \sum_{k=1}^K \delta(k = y_p) z_{p,k}(\mathbf{x}; \theta_U). \quad (4)$$

Here $\delta(\cdot)$ is the indicator function, which equals 1 if the input is true and 0 otherwise; K is the number of classes; $z_{p,k}$ is the unary network output value that corresponds to the p -th node and the k -th class. θ_U is the network parameters for the potential function U , which we need to learn. The dimension of the unary network output for one node is K .

3.2 Pairwise potential functions

We formulate the pairwise potential function as follows:

$$V(y_p, y_q, \mathbf{x}; \theta_V) = \sum_{k=1}^K \sum_{j=1}^K \delta(k = y_p) \delta(j = y_q) z_{p,q,k,j}(\mathbf{x}; \theta_V). \quad (5)$$

Here $z_{p,q,k,j}$ is the pairwise network output. It is the cost value for the node pair (p, q) when they are labeled with the class value (k, j) . θ_V is the corresponding CNN parameters for the pairwise potential function V , which we need to learn. The dimension of the pairwise network output for one pairwise connection is: K^2 .

3.3 Prediction

To predict the labeling of a new image, we solve the maximum a posteriori (MAP) inference problem:

$$\mathbf{y}^* = \operatorname{argmax}_{\mathbf{y}} P(\mathbf{y}|\mathbf{x}). \quad (5)$$

Our CRF graph does not form a tree structure, hence we need to apply approximate inference algorithm to solve the above MAP problem. Here we have applied an efficient message passing algorithm which is based on the mean field approximation [24], [14]. The mean field approximation constructs a simpler distribution $Q(\mathbf{y})$, e.g., a product of independent marginals: $Q(\mathbf{y}) = \prod Q_p(y_p)$, which minimizes the KL-divergence between the CRF distribution $P(\mathbf{y})$ and $Q(\mathbf{y})$.

3.4 CRF training

A common approach for CRF learning is to maximise the likelihood, or equivalently minimising negative log-likelihood. The negative log-likelihood for one image is written as:

$$-\log P(\mathbf{y}|\mathbf{x}; \theta) = E(\mathbf{y}, \mathbf{x}; \theta) + \log Z(\mathbf{x}; \theta). \quad (6)$$

Adding regularization to θ , the optimization problem for CRF learning is written as:

$$\min_{\theta} \frac{\lambda}{2} \|\theta\|_2^2 - \sum_{i=1}^N \log P(\mathbf{y}^{(i)}|\mathbf{x}^{(i)}; \theta). \quad (7)$$

Here $\mathbf{x}^{(i)}$, $\mathbf{y}^{(i)}$ denote the i -th training image and the corresponding segmentation mask; N is the number of training images; λ is weight decay parameter. The above optimization can be further written as:

$$\min_{\theta} \frac{\lambda}{2} \|\theta\|_2^2 + \sum_{i=1}^N \left[E(\mathbf{y}^{(i)}, \mathbf{x}^{(i)}; \theta) + \log Z(\mathbf{x}^{(i)}; \theta) \right]. \quad (8)$$

We can apply gradient-based method to optimize the above problem for learning θ . The gradient of the partition function is:

$$\begin{aligned}
& \nabla_{\theta} \log Z(\mathbf{x}; \theta) \\
&= \nabla_{\theta} \log \sum_{\mathbf{y}} \exp[-E(\mathbf{y}, \mathbf{x})] \\
&= \sum_{\mathbf{y}} \frac{\exp[-E(\mathbf{y}, \mathbf{x}; \theta)]}{\sum_{\mathbf{y}'} \exp[-E(\mathbf{y}', \mathbf{x}; \theta)]} \nabla_{\theta}[-E(\mathbf{y}, \mathbf{x}; \theta)] \\
&= - \sum_{\mathbf{y}} P(\mathbf{y}|\mathbf{x}; \theta) \nabla_{\theta} E(\mathbf{y}, \mathbf{x}; \theta) \\
&= - \mathbb{E}_{\mathbf{y} \sim P(\mathbf{y}|\mathbf{x}; \theta)} \nabla_{\theta} E(\mathbf{y}, \mathbf{x}; \theta) \tag{9}
\end{aligned}$$

With the above result, the gradient of the objective function in (8) is written as:

$$\begin{aligned}
\nabla_{\theta} L(\theta) = & \lambda \theta + \sum_{i=1}^N \left[\nabla_{\theta} E(\mathbf{y}^{(i)}, \mathbf{x}^{(i)}; \theta) \right. \\
& \left. - \mathbb{E}_{\mathbf{y} \sim P(\mathbf{y}^{(i)}|\mathbf{x}^{(i)}; \theta)} \nabla_{\theta} E(\mathbf{y}^{(i)}, \mathbf{x}^{(i)}; \theta) \right]. \tag{10}
\end{aligned}$$

The energy function $E(\mathbf{y}, \mathbf{x}; \theta)$ is constructed from CNNs. The gradient $\nabla_{\theta} E(\mathbf{y}, \mathbf{x}; \theta)$ can be easily computed as in conventional CNNs and back propagation is applied. However, the partition function Z brings trouble for optimization. Generally the size of the output space \mathcal{Y} is exponentially increased in the number of nodes, which prohibits the direct calculation of Z and its gradient. If the graph is tree-structured, we can apply brief propagation for exact calculation of the gradient of the partition function. Otherwise, approximation is required. For non tree-structured graphs, direct gradient calculation is generally computationally very expensive. The CRF graph we considered here does not form a tree structure.

Note that typically millions of stochastic gradient descent (SGD) iterations are required for training CNNs. Assume that 1 million iterations are performed such that in total 1 million times of inference is needed. If each inference takes 1 second, the time spent on inference alone would be nearly 12 days. We need efficient methods that avoid repeated inference in training.

3.5 Piecewise training of CRFs

Instead of directly solving the optimization in (8) for CRF learning, we here apply an approximate CRF learning method. In the literature, there are two popular types of learning methods which approximate the original CRF objective by decomposing the graph: one is pseudo-likelihood learning [25]. It has been applied in the literature, for example, decision tree fields [26] and regression tree fields [27]. The other one is piecewise learning [4], which is applied in the work [4], [23].

We first consider piecewise training for CRF and CNN joint learning. In CRF piecewise training, the original graph is decomposed into a number of disjointed small graphs. Each small graph only involves one potential

function. Hence the origin loss function is approximated by a loss function that is easy to optimize. For piecewise training, the conditional distribution is written as:

$$P(\mathbf{y}|\mathbf{x}) = \prod_{U \in \mathcal{U}} \prod_{p \in \mathcal{N}_U} P_U(y_p|\mathbf{x}) \prod_{V \in \mathcal{V}} \prod_{(p,q) \in \mathcal{S}_V} P_V(y_p, y_q|\mathbf{x}). \tag{11}$$

Here $P_U(y_p|\mathbf{x})$ is the distribution function constructed from the potential function U . Likewise, $P_V(\mathbf{y}|\mathbf{x})$ is constructed by the pairwise potential function V . P_U and P_V are written as:

$$P_U(y_p|\mathbf{x}) = \frac{\exp[-U(y_p, \mathbf{x})]}{\sum_{y'_p} \exp[-U(y'_p, \mathbf{x})]}, \tag{12}$$

$$P_V(y_p, y_q|\mathbf{x}) = \frac{\exp[-V(y_p, y_q, \mathbf{x})]}{\sum_{y'_p, y'_q} \exp[-V(y'_p, y'_q, \mathbf{x})]}. \tag{13}$$

The log-likelihood for piecewise training is written as:

$$\begin{aligned}
\log P(\mathbf{y}|\mathbf{x}) = & \sum_{U \in \mathcal{U}} \sum_{p \in \mathcal{N}_U} \log P_U(y_p|\mathbf{x}) \\
& + \sum_{V \in \mathcal{V}} \sum_{(p,q) \in \mathcal{S}_V} \log P_V(y_p, y_q|\mathbf{x}). \tag{14}
\end{aligned}$$

The optimization problem for piecewise training is to minimize the negative log likelihood with regularization, which is written as:

$$\begin{aligned}
\min_{\theta} \frac{\lambda}{2} \|\theta\|_2^2 - & \sum_{i=1}^N \left[\sum_{U \in \mathcal{U}} \sum_{p \in \mathcal{N}_U^{(i)}} \log P_U(y_p|\mathbf{x}^{(i)}; \theta_U) \right. \\
& \left. + \sum_{V \in \mathcal{V}} \sum_{(p,q) \in \mathcal{S}_V^{(i)}} \log P_V(y_p, y_q|\mathbf{x}^{(i)}; \theta_V) \right]. \tag{15}
\end{aligned}$$

The above objective is decomposed over nodes and edges, hence it can be efficiently optimized.

3.6 Pseudo-likelihood training of CRFs

CRF pseudo-likelihood training [25] is an alternative to piecewise training for efficient CRF learning, which has been applied in decision tree fields [26] and regression tree fields [27]. Pseudo-likelihood training approximates the original likelihood by the product of the likelihood functions defined on individual nodes. The likelihood function for one node is conditioned on all remaining nodes. The likelihood function for each node can be independently optimized. The conditional likelihood for pseudo-likelihood training is written as:

$$P(\mathbf{y}|\mathbf{x}) = \prod_{p \in \mathcal{N}} P(y_p|\bar{\mathbf{y}}_p, \mathbf{x}). \tag{16}$$

Here \bar{y}_p is the output variables exclude the y_p . The log-likelihood is written as:

$$\begin{aligned} \log P(\mathbf{y}|\mathbf{x}; \boldsymbol{\theta}) &= \log \prod_{p \in \mathcal{N}} P(y_p | \bar{y}_p, \mathbf{x}; \boldsymbol{\theta}) \\ &= \log \prod_{p \in \mathcal{N}} \frac{1}{Z_p(\mathbf{x}; \boldsymbol{\theta})} \exp[-E(\mathbf{y}, \mathbf{x}; \boldsymbol{\theta})] \\ &= \sum_{p \in \mathcal{N}} -E(y_p, \bar{y}_p, \mathbf{x}; \boldsymbol{\theta}) - \log Z_p(\mathbf{x}; \boldsymbol{\theta}). \end{aligned} \quad (17)$$

Here Z_p is the partition function in the likelihood function for the node p , which is written as:

$$Z_p(\mathbf{x}; \boldsymbol{\theta}) = \sum_{y_p} \exp[-E(y_p, \bar{y}_p, \mathbf{x}; \boldsymbol{\theta})]. \quad (18)$$

The optimization problem for pseudo-likelihood training is to minimize the negative log-likelihood with regularization, which is written as:

$$\min_{\boldsymbol{\theta}} \frac{\lambda}{2} \|\boldsymbol{\theta}\|_2^2 + \sum_{i=1}^N \sum_{p \in \mathcal{N}^{(i)}} \left[E(y_p^{(i)}, \bar{y}_p^{(i)}, \mathbf{x}^{(i)}; \boldsymbol{\theta}) + \log Z_p(\mathbf{x}^{(i)}; \boldsymbol{\theta}) \right]. \quad (19)$$

For CNNs and CRFs joint training, we need to calculate the gradient of the above objective. The gradient of $E(\cdot)$ can be efficiently calculated by network back-propagation. Note that Z_p only involves one output variable, hence it is efficient to calculate Z_p and its gradient. The gradient of $\log Z_p(\mathbf{x}; \boldsymbol{\theta})$ is:

$$\begin{aligned} \nabla_{\boldsymbol{\theta}} \log Z_p(\mathbf{x}; \boldsymbol{\theta}) &= \nabla_{\boldsymbol{\theta}} \log \sum_{y_p} \exp[-E(y_p, \bar{y}_p, \mathbf{x})] \\ &= - \sum_{y_p} \frac{\exp[-E(y_p, \bar{y}_p, \mathbf{x}; \boldsymbol{\theta})]}{\sum_{y'_p} \exp[-E(y'_p, \bar{y}_p, \mathbf{x}; \boldsymbol{\theta})]} \nabla_{\boldsymbol{\theta}} E(\mathbf{y}, \mathbf{x}; \boldsymbol{\theta}) \\ &= - \sum_{y_p} P(y_p | \bar{y}_p, \mathbf{x}; \boldsymbol{\theta}) \nabla_{\boldsymbol{\theta}} E(\mathbf{y}, \mathbf{x}; \boldsymbol{\theta}). \end{aligned} \quad (20)$$

Our initial experiment results show that pseudo-likelihood training converges slower than the piecewise training, but with comparable accuracy. Therefore in the sequel, we report the results obtained by piecewise training.

4 EXPERIMENTS

We evaluate our method on the PASCAL VOC 2012 dataset [28] which consists of 20 object categories and one background category. This dataset contains 1464 images in the training set, 1449 images in the validation set and 1456 images in the test set. Following the setting in [8], [3], the training set is augmented by extra annotations provided in [29], which results in 10582 training images. We evaluate our method both in the validation set and the test set. We compare to several recent methods which represent the state-of-the-art performance on

semantic segmentation. The segmentation performance is measured by the intersection-over-union score [28].

4.1 Implementation details

The first 5 convolution blocks in our networks are initialized from the VGG-16 model [20] which is trained on ImageNet [30]. This model is also used in most comparing methods. In the 6th convolution block, the first convolution layer is initialized from the first fully connected layer in VGG-16. All remaining layers are randomly initialized. All layers are trained using back-propagation. The learning rate for randomly initialized layers is set to 0.001. For VGG-16 initialized layers we use a smaller learning rate: 0.0001. We use 3 scales for the input image: 1.2, 0.8 and 0.4. The weight decay parameter is set to 0.0005; the momentum parameter is set to 0.9.

We observe that piecewise training is able to achieve slightly better performance, but faster convergence than pseudo-likelihood training. Thus we apply piecewise training throughout our experiments.

The CRF graph is constructed based on the size of the largest feature map which is generated by the last convolution block. One node in the graph corresponds to one spatial position in this feature map. For each node we use a rectangle box to specify the neighbourhood range for pairwise connections. As illustrated in Fig. 1, we are using 3 types of pairwise potential functions each of which has a different setting of the neighborhood range box. The range box size is adapted to the size of the input image.

We denote by a the length of the shortest edge of the largest feature map. For the first pairwise potential ‘‘Pairwise-1’’, the range box size is $0.4a \times 0.4a$; the range box is centered on the node. For the second pairwise potential: ‘‘Pairwise-2’’, the range box size is $0.3a \times 0.4a$; the bottom edge of the range box is centered on the node. For the third pairwise potential: ‘‘Pairwise-3’’, the range box size is $0.4a \times 0.3a$; the top edge of the range box is centered on the node.

Due to the operators of convolution and pooling strides, the final convolution feature map is smaller than the size of the input image, thus we need to perform down-sampling of the ground-truth for training and up-sampling the prediction mask. In the training stage, the ground truth segmentation mask is resized to match the largest feature map by nearest neighbor down-sampling. In the prediction stage, the prediction confidence score map is up-sampled by bilinear interpolation to match the size of the input image.

4.2 Evaluation of different settings

We first evaluate our method with different parameter settings. Table 1 shows the results on the PASCAL VOC 2012 validation set. We compare to a number of recent methods which have reported results on the validation set.

TABLE 2 – Individual category results of our method on the PASCAL VOC 2012 validation set using different settings.

| method | mean | aero | bike | bird | boat | bottle | bus | car | cat | chair | cow | table | dog | horse | mbike | person | potted | sheep | sofa | train | tv |
|--------------|------|-------------|-------------|-------------|-------------|-------------|-------------|-------------|-------------|-------------|-------------|-------------|-------------|-------------|-------------|-------------|-------------|-------------|-------------|-------------|-------------|
| unary-1scale | 58.3 | 71.2 | 32.4 | 66.9 | 53.5 | 55.8 | 72.9 | 70.8 | 73.1 | 25.3 | 54.6 | 38.5 | 64.1 | 55.3 | 66.9 | 73.4 | 40.6 | 61.3 | 30.2 | 69.5 | 58.1 |
| unary | 65.5 | 76.3 | 35.7 | 74.3 | 58.8 | 70.4 | 85.3 | 81.3 | 79.1 | 30.1 | 62.3 | 43.5 | 69.9 | 67.3 | 73.7 | 77.9 | 49.9 | 71.8 | 36.6 | 76.7 | 62.9 |
| pairwise-1 | 66.1 | 79.6 | 33.8 | 76.8 | 57.8 | 67.6 | 87.8 | 81.5 | 80.7 | 32.1 | 62.6 | 50.1 | 75.5 | 66.1 | 71.3 | 77.7 | 50.0 | 69.7 | 35.0 | 76.6 | 64.6 |
| full | 70.2 | 87.2 | 36.9 | 81.9 | 62.7 | 74.3 | 89.8 | 83.8 | 83.3 | 33.2 | 65.4 | 51.3 | 78.8 | 73.2 | 78.6 | 81.7 | 54.5 | 77.3 | 38.5 | 81.3 | 68.6 |

TABLE 3 – Individual category results on the PASCAL VOC 2012 test set. Our method performs the best.

| method | mean | aero | bike | bird | boat | bottle | bus | car | cat | chair | cow | table | dog | horse | mbike | person | potted | sheep | sofa | train | tv |
|-----------------|-------------|-------------|-------------|-------------|-------------|-------------|-------------|-------------|-------------|-------------|-------------|-------------|-------------|-------------|-------------|-------------|-------------|-------------|-------------|-------------|-------------|
| DeepLab-CRF [3] | 66.4 | 78.4 | 33.1 | 78.2 | 55.6 | 65.3 | 81.3 | 75.5 | 78.6 | 25.3 | 69.2 | 52.7 | 75.2 | 69.0 | 79.1 | 77.6 | 54.7 | 78.3 | 45.1 | 73.3 | 56.2 |
| FCN-8s [2] | 62.2 | 76.8 | 34.2 | 68.9 | 49.4 | 60.3 | 75.3 | 74.7 | 77.6 | 21.4 | 62.5 | 46.8 | 71.8 | 63.9 | 76.5 | 73.9 | 45.2 | 72.4 | 37.4 | 70.9 | 55.1 |
| ours | 70.7 | 88.0 | 37.5 | 75.8 | 57.0 | 72.0 | 88.3 | 82.8 | 79.3 | 33.5 | 71.2 | 55.9 | 78.5 | 77.7 | 81.7 | 82.7 | 55.9 | 80.4 | 49.8 | 78.1 | 65.8 |

TABLE 1 – Segmentation results on the PASCAL VOC 2012 val set.

We evaluate our method with different settings, and compare against several recent methods with available results on the validation set. Our full model performs the best.

| method | training set | # train | IoU val set |
|-------------------|------------------|---------|-------------|
| ours-unary-1scale | VOC extra | 10k | 58.3 |
| ours-unary | VOC extra | 10k | 65.5 |
| ours-pairwise-1 | VOC extra | 10k | 66.1 |
| ours-pairwise-2 | VOC extra | 10k | 65.6 |
| ours-pairwise-3 | VOC extra | 10k | 65.8 |
| ours-1u-3p | VOC extra | 10k | 67.4 |
| ours-full | VOC extra | 10k | 70.2 |
| Zoom-out [19] | VOC extra | 10k | 63.5 |
| Deep-struct [15] | VOC extra | 10k | 64.1 |
| DeepLab [3] | VOC extra | 10k | 59.8 |
| DeepLab-CRF [3] | VOC extra | 10k | 63.7 |
| BoxSup [9] | VOC extra | 10k | 63.8 |
| BoxSup [9] | VOC extra + COCO | 133k | 68.1 |

The first two rows show the results of our unary-only models using 1 image scale and 3 image scales (denoted by “ours-unary-1scale” and “ours-unary” in the result table). Clearly the 3-scales setting has achieved much better performance. Unless otherwise specified, in the sequel our method uses 3 image scales.

We also evaluate the performance of only using one type of potential function. It shows that our method using a single type of potential function already outperforms other methods which use the same augmented PASCAL VOC dataset provided in [29]. By combining all potential functions, the performance of our method (denoted by “ours-1u-3p”) is further improved. This result shows that the learnt potential functions are capable of capturing different kinds of information.

Finally, to further refine our predictions, we apply the post-processing technique proposed in [14], which has also been used in the comparing method DeepLab [3] and BoxSup [9]. This post-processing step incorporates more low-level information, resulting in sharp prediction on object boundaries. Our final performance (denoted by “ours-full” in the result table) achieves 70.2 IoU score on the validation set, which is significantly better than all other compared methods.

DeepLab-CRF is the method DeepLab without using the dense CRF method in [14] for post-processing. Our method outperforms DeepLab and DeepLab-CRF by a large margin. The recent method BoxSup [9] explores

TABLE 4 – Segmentation results on the PASCAL VOC 2012 test set.

Compared to methods that use the same augmented PASCAL VOC dataset, our method performs the best. Compared to methods trained on extra COCO dataset, our method achieves on par performance, while using much less training data.

| method | training set | # train | IoU test set |
|------------------|------------------|---------|--------------|
| Zoom-out [19] | VOC extra | 10k | 64.4 |
| FCN-8s [2] | VOC extra | 10k | 62.2 |
| SDS [8] | VOC extra | 10k | 51.6 |
| CRF-RNN [16] | VOC extra | 10k | 65.2 |
| DeepLab-CRF [3] | VOC extra | 10k | 66.4 |
| DeepLab-CRF [32] | VOC extra + COCO | 133k | 70.4 |
| BoxSup [9] | VOC extra + COCO | 133k | 71.0 |
| ours | VOC extra | 10k | 70.7 |

the COCO dataset together with the VOC augmented dataset. The COCO dataset [31] consists of 133K images which is much larger than the augmented VOC dataset. The result shows that our method still outperforms BoxSup which is trained on the joint dataset of COCO and augmented PASCAL VOC.

The detailed results of our method for each category is shown in Table 2. We compare the performance of different settings. “unary-1scale” is the unary-only model with one image scale; “unary” is the unary-only model with 3 image scales; “pairwise-1” is the model only use the “Pairwise-1” potential function which captures the surrounding patch relations; “full” indicates our final model. It shows that all categories benefit from using 3 image scales. The unary model and pairwise model show different preferences on categories. Bold-faced numbers for each category in the result table indicate the model with better performance. The categories: dining table, dog, aeroplane, TV/monitor, bird, bus and chair gain significantly benefits from the pairwise model which explores neighborhood relations.

Some segmentation examples are demonstrated in Fig. 5; and a few failed examples are shown in Fig. 6.

4.3 Comparison on the test set

We compare with a number of recent methods which have competitive performances. Table 4 shows the results on the PASCAL VOC 2012 test set. The ground truth labels are not available for the test set. We evaluate our method through the PASCAL VOC evaluation

server. We achieve a very impressive result on the test set: 70.7 IoU score¹, which is the best performance compared to methods that use the same augmented PASCAL VOC dataset provided in [29]. We also include the comparison with methods that trained on the much larger COCO dataset (133K training images). Our performance is on a par with these methods, while our method uses much less training images.

The results for each category is shown in Table 3. We compare with two most relevant methods: DeepLab-CRF [3] and FCN-8s [2], which are fully-CNN based methods and transfer layers from the same VGG-16 model. Our method performs the best in almost all categories.

5 CONCLUSIONS

We have proposed a method which jointly learns FCNNs and CRFs to explore *complex* contextual information for semantic image segmentation. Our competitive performance on the PASCAL VOC 2012 dataset has validated its effectiveness and usefulness. Bear in mind that the proposed DCRFs are general and can be applied to many other vision tasks, which is our future work.

1. Obtained by submitting results to the PASCAL VOC evaluation server: <http://host.robots.ox.ac.uk:8080/anonymous/VNSFVL.html>



Fig. 5 – Some segmentation examples on the PASCAL VOC 2012 validation set.

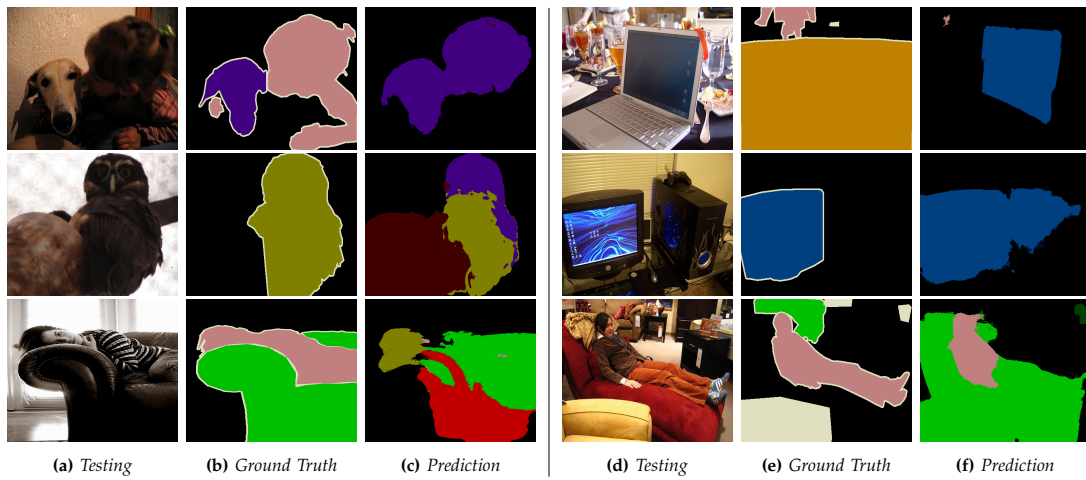


Fig. 6 – *Some examples with weak performance.*

REFERENCES

- [1] C. Farabet, C. Couprie, L. Najman, and Y. LeCun, "Learning hierarchical features for scene labeling," *IEEE T. Pattern Analysis Mach. Intelli.*, 2013.
- [2] J. Long, E. Shelhamer, and T. Darrell, "Fully convolutional networks for semantic segmentation," in *Proc. IEEE Conf. Comp. Vis. Pattern Recogn.*, 2015.
- [3] L. Chen, G. Papandreou, I. Kokkinos, K. Murphy, and A. L. Yuille, "Semantic image segmentation with deep convolutional nets and fully connected CRFs," 2014. [Online]. Available: <http://arxiv.org/abs/1412.7062>
- [4] C. A. Sutton and A. McCallum, "Piecewise training for undirected models," in *Proc. Conf. Uncertainty Artificial Intelli*, 2005.
- [5] A. Krizhevsky, I. Sutskever, and G. E. Hinton, "ImageNet classification with deep convolutional neural networks," in *Proc. Adv. Neural Info. Process. Syst.*, 2012.
- [6] R. B. Girshick, J. Donahue, T. Darrell, and J. Malik, "Rich feature hierarchies for accurate object detection and semantic segmentation," in *Proc. IEEE Conf. Comp. Vis. Pattern Recogn.*, 2014.
- [7] J. Tompson, A. Jain, Y. LeCun, and C. Bregler, "Joint training of a convolutional network and a graphical model for human pose estimation," in *Proc. Adv. Neural Info. Process. Syst.*, 2014.
- [8] B. Hariharan, P. Arbeláez, R. Girshick, and J. Malik, "Simultaneous detection and segmentation," in *Proc. European Conf. Computer Vision*, 2014.
- [9] J. Dai, K. He, and J. Sun, "BoxSup: Exploiting bounding boxes to supervise convolutional networks for semantic segmentation," 2015. [Online]. Available: <http://arxiv.org/abs/1503.01640>
- [10] D. Eigen, D. Krishnan, and R. Fergus, "Restoring an image taken through a window covered with dirt or rain," in *Proc. Int. Conf. Comp. Vis.*, 2013.
- [11] C. Dong, C. C. Loy, K. He, and X. Tang, "Learning a deep convolutional network for image super-resolution," in *Proc. Eur. Conf. Comp. Vis.*, 2014.
- [12] D. Eigen, C. Puhrsch, and R. Fergus, "Depth map prediction from a single image using a multi-scale deep network," in *Proc. Adv. Neural Info. Process. Syst.*, 2014.
- [13] F. Liu, C. Shen, and G. Lin, "Deep convolutional neural fields for depth estimation from a single image," in *Proc. IEEE Conf. Comp. Vis. Pattern Recogn.*, 2015.
- [14] P. Krähenbühl and V. Koltun, "Efficient inference in fully connected CRFs with Gaussian edge potentials," in *Proc. Adv. Neural Info. Process. Syst.*, 2012.
- [15] A. G. Schwing and R. Urtasun, "Fully connected deep structured networks," 2015. [Online]. Available: <http://arxiv.org/abs/1503.02351>
- [16] S. Zheng, S. Jayasumana, B. Romera-Paredes, V. Vineet, Z. Su, D. Du, C. Huang, and P. Torr, "Conditional random fields as recurrent neural networks," 2015. [Online]. Available: <http://arxiv.org/abs/1502.03240>
- [17] F. Liu, C. Shen, G. Lin, and I. Reid, "Learning depth from single monocular images using deep convolutional neural fields," 2015. [Online]. Available: <http://arxiv.org/abs/1502.07411>
- [18] L.-C. Chen, A. G. Schwing, A. L. Yuille, and R. Urtasun, "Learning deep structured models," 2014. [Online]. Available: <http://arxiv.org/abs/1407.2538>
- [19] M. Mostajabi, P. Yadollahpour, and G. Shakhnarovich, "Feedforward semantic segmentation with zoom-out features," 2014. [Online]. Available: <http://arxiv.org/abs/1412.0774>
- [20] K. Simonyan and A. Zisserman, "Very deep convolutional networks for large-scale image recognition," 2014. [Online]. Available: <http://arxiv.org/abs/1409.1556>
- [21] J. Winn and J. Shotton, "The layout consistent random field for recognizing and segmenting partially occluded objects," in *Proc. IEEE Conf. Comp. Vis. Pattern Recogn.*, 2006.
- [22] D. Heesch and M. Petrou, "Markov random fields with asymmetric interactions for modelling spatial context in structured scene labelling," *Journal of Signal Processing Systems*, 2010.
- [23] A. Kolesnikov, M. Guillaumin, V. Ferrari, and C. H. Lampert, "Closed-form training of conditional random fields for large scale image segmentation," in *Proc. Eur. Conf. Comp. Vis.*, 2014.
- [24] D. Koller and N. Friedman, *Probabilistic graphical models: principles and techniques*. MIT Press, 2009.
- [25] J. Besag, "Efficiency of pseudolikelihood estimation for simple Gaussian fields," *Biometrika*, 1977.
- [26] S. Nowozin, C. Rother, S. Bagon, T. Sharp, B. Yao, and P. Kohli, "Decision tree fields," in *Proc. Int. Conf. Comp. Vis.*, 2011.
- [27] J. Jancsary, S. Nowozin, T. Sharp, and C. Rother, "Regression tree fields: an efficient, non-parametric approach to image labeling problems," in *Proc. IEEE Conf. Comp. Vis. Pattern Recogn.*, 2012.
- [28] M. Everingham, L. Van Gool, C. K. Williams, J. Winn, and A. Zisserman, "The pascal visual object classes (voc) challenge," *Int. J. Comp. Vis.*, 2010.
- [29] B. Hariharan, P. Arbeláez, L. D. Bourdev, S. Maji, and J. Malik, "Semantic contours from inverse detectors," in *Proc. Int. Conf. Comp. Vis.*, 2011.
- [30] J. Deng, W. Dong, R. Socher, L.-J. Li, K. Li, and L. Fei-Fei, "Imagenet: A large-scale hierarchical image database," in *Proc. IEEE Conf. Comp. Vis. Pattern Recogn.*, 2009.
- [31] T.-Y. Lin, M. Maire, S. Belongie, J. Hays, P. Perona, D. Ramanan, P. Dollár, and C. L. Zitnick, "Microsoft COCO: Common objects in context," in *Proc. Eur. Conf. Comp. Vis.*, 2014.
- [32] G. Papandreou, L.-C. Chen, K. Murphy, and A. L. Yuille, "Weakly-and semi-supervised learning of a DCNN for semantic image segmentation," 2015. [Online]. Available: <http://arxiv.org/abs/1502.02734>